



ChemComm

**Determining role of structural flexibility on catalytic activity
of conductive 2D layered metal-organic frameworks**

Journal:	<i>ChemComm</i>
Manuscript ID	CC-COM-11-2020-007430.R1
Article Type:	Communication

SCHOLARONE™
Manuscripts

Cite this: DOI: 00.0000/xxxxxxxxxx

Determining role of structural flexibility on catalytic activity of conductive 2D layered metal–organic frameworks[†]Mohammad R. Momeni,^{*a} Zeyu Zhang,^a and Farnaz A. Shakib^{*a}Received Date
Accepted Date

DOI: 00.0000/xxxxxxxxxx

A combined quantum mechanics and classical molecular dynamics approach is used to unravel the effects of structural deformations and heterogeneity on catalytic activity of 2D π -stacked layered metal-organic frameworks. Theory predicts that the flexible nature of these materials creates a complex array of catalytically active sites for oxidative dehydrogenation of propane. Using an ensemble approach and oxygen bond formation energy, as an excellent probe, we investigate the catalytic activity down to the single active site level.

Recently introduced 2D π -stacked layered metal-organic frameworks (MOFs) offer record breaking electrical conductivity along with permanent porosity and high surface area.^{1–4} Combined with their low dimensionality for compact device implementation, this new class of 2D materials has inspired development of MOF-based batteries and supercapacitors^{5–12} as well as potentiometric and chemiresistive sensors.^{11,13,14} Having 1-D channels with ≈ 20 Å diameters, they allow penetration of target analytes making them perfect choices for adsorption, separation and catalysis (Figure 1). In spite of all these merits, their catalytic utilization is limited by the lack of understanding of the intrinsic MOF structure and dynamics and host-guest interactions at the single catalytic active site level. Recently, we have unravelled a range of dynamical motions in two archetypical 2D MOFs, $\text{Cu}_3(\text{HHTTP})_2$ and $\text{Co}_3(\text{HHTTP})_2$, where HHTTP=hexahydroxytriphenylene, and have shown how these motions lead to creation of deformation sites in the latter.¹⁵ This dynamic flexibility was shown to drastically influence interaction of the secondary building units (SBUs) of these MOFs with water molecules. Similarly, it is anticipated that the flexible nature of 2D MOFs could potentially create different catalytic ac-

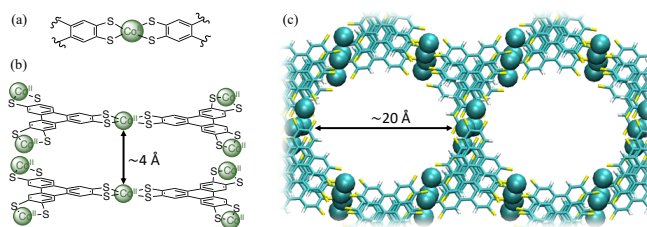


Fig. 1 Conductive 2D π -stacked layered $\text{Co}_3(\text{HHTTP})_2$ (HHTTP=hexahydroxytriphenylene) MOF. Schematic representation of (a) tetra-coordinated metal node creating (b) an extended layer via tri-topic HHTTP linkers, and (c) crystal structure of the extended material highlighting the hexagonal array of the 1D channels.

tive sites with a wide range of reactivity for any desired reaction. The importance of the presence of deformations and defects as well as open-metal sites on catalytic activity of different MOFs is highlighted before.^{16–20} Single-atom Co-deposited MOFs are shown to be excellent heterogeneous catalysts in catalytic conversion of propane to value-added chemicals under mild conditions.^{21,22} Herein, oxidative dehydrogenation (ODH) of propane using N_2O as oxidizing agent^{23,24} is adopted for studying the effect of structural deformations on catalytic activity of the coordinatively unsaturated Co sites in $\text{Co}_3(\text{HHTTP})_2$, where HHTTP=hexathiotriphenylene. Several experimental studies have used N_2O as an excellent oxidant for partial oxidation of different alkanes.^{25–27} Also, the selectivity and mechanism by which N_2O is activated, via the O-mode and not the N-mode, especially for light hydrocarbons is already well-established.^{28,29} Here, we employ a combined classical molecular dynamics (MD) and quantum mechanics approach to illustrate different levels of heterogeneity and disorder in equilibrated 2D MOFs, painting a realistic picture of catalytic activity of $\text{Co}_3(\text{HHTTP})_2$ compared to pristine structures obtained from *static* electronic structure calculations. We show that cobalt–oxygen bond formation energy can be used as an excellent probe of catalytic reactivity at the single active site level.

The large number of atoms and the flexible nature of 2D MOFs

^a Department of Chemistry and Environmental Science, New Jersey Institute of Technology, Newark 07102, NJ United States, E-mail: momeni@njit.edu, shakkib@njit.edu

[†] Electronic Supplementary Information (ESI) available: Details of our flexible *ab initio* force field, results of our classical MD simulations, details of the periodic and cluster electronic structure calculations as well as XYZ coordinates of all studied systems. See DOI: 00.0000/00000000.

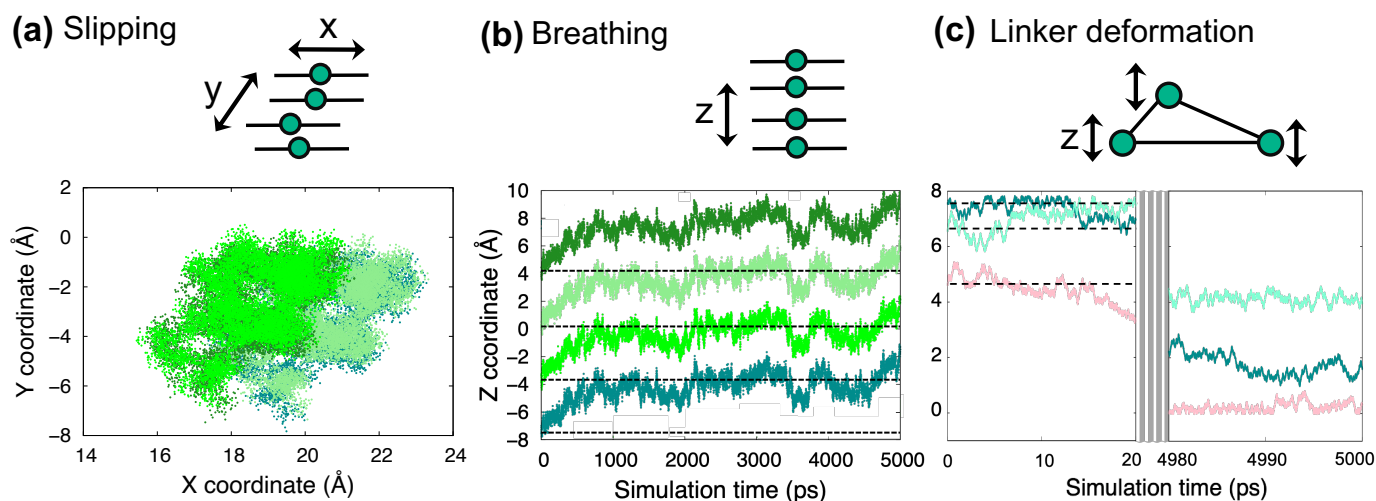


Fig. 2 Three characteristic dynamical motions in $\text{Co}_3(\text{HTTP})_2$ with schematic representations at the top, and statistical results over the entire 5 ns trajectories at the bottom. (a) slipping and (b) breathing movement of four adjacent layers using the position of four different Co atoms, green circles in the scheme, as geometrical indicator. Horizontal dashed lines indicate the initial positions from our 0 K *ab initio* optimized structure. (c) Planarity deformation of organic linkers represented with the vertical movement of three Co atoms attached to the same linker, represented with a triangle.

leads to huge computational cost if *ab initio* molecular dynamics (AIMD) were to be used, making force field based techniques more suitable for this task. Therefore, we have carried out classical MD simulations on an extended $2 \times 2 \times 2$ model of $\text{Co}_3(\text{HTTP})_2$ MOF based on our newly-developed *ab initio* force field (FF) parameterized against highly accurate $\omega\text{B97M-v}/\text{def2-TZVP}^{30}$ density functional. This FF allows nanosecond scale simulations, far beyond capabilities of AIMD simulations, while reproducing similar accuracy in capturing the intra- and interlayer framework deformation and heterogeneity. Details of developing and validating the force field against experimental and *ab initio* data, and comparison of structural deformations between our approach and AIMD, is provided in the Supporting Information (SI) (sections S1–S3). Here, we first illustrate the effect of dynamical motions on inducing structural deformations and heterogeneity by comparing the results of MD simulations at 293 K to those of *static* electronic structure calculations at 0 K. Figure 2 illustrates three classes of dynamical motions during 5 ns simulation time including slipping of layers in xy plane, *i.e.* along “*a*” and “*b*” vectors, expansion or contraction of interlayer distance in z direction, *i.e.* breathing along the “*c*” vector, and deformation of individual organic linkers. Both, 0 K PBE-D3/DZVP-MOLOPT optimized and 293 K MD equilibrated frameworks show layers that are slipped relative to each other in the xy plane. The Co-Co-Co-Co dihedral angle as depicted at the top of Figure 2, $\angle da$, is a good geometrical descriptor to quantify the degree of slipping disorder. There are 12 such angles within the cell. While $\angle da$ of the 0 K optimized MOF has a narrow range of 179.4° – 180.0° , the calculated range of $\angle da$ for equilibrated MOF at 293 K is 170.0° – 177.2° showing a higher degree of slipping deformation. Figure 2a shows that slipping of layers is a constant motion during 5 ns simulation time. This observation is in agreement with previous studies where slipping of layers, mostly to form an AB slipped-parallel stacking pattern, has been confirmed in various 2D MOFs includ-

ing $\text{Co}_3(\text{HTTP})_2$.^{4,14,31–34} The dashed lines in Figure 2b represent the 0 K optimized positions of $\text{Co}_3(\text{HTTP})_2$ layers in z direction. As can be seen, all layers have a very wide range of movements in z direction during 5 ns simulation time. This can have a considerable impact on catalytic activity of the 2D MOF because a larger interlayer space further exposes the coordinatively unsaturated open-Co sites to the incoming analytes. Dashed lines in Figure 2c represent the position of three metal nodes connected to the same organic linker as obtained from the 0 K optimized structure. As can be seen, by the end of the MD simulation at 293 K the organic linkers are completely twisted which combined with slipping of the layers has a significant effect on the coordination environment of the open-Co sites. In this very flexible architecture, metal nodes show both square planar and tetrahedral coordination environments which adds another layer of heterogeneity to the structure and function of 2D MOFs. Next, we address the impacts of these structural deformations on catalytic activity of $\text{Co}_3(\text{HTTP})_2$ in ODH of propane as a case study.

Figure 3 illustrates the 4-step mechanistic cycle for N_2O -assisted ODH of propane on $\text{Co}_3(\text{HTTP})_2$, similar to the mechanism suggested by Barona et al. for PCN-250 and Verma et al. for $\text{Fe}_2(\text{dobdc})$,²⁸ which starts with binding of the oxidizing agent N_2O to the open-metal sites resulting in formation of a metal-oxo bond and N_2 liberation (**step 1**, rate-determining step). It is then followed by C-H bond activation of the secondary hydrogen of propane (**step 2**) resulting in either formation of propanol or another C-H activation to form terminal water and propene. Having found a strong correlation ($R^2 = 0.98$) between the N_2O activation energy barriers and the metal-oxygen bond formation energies, Barona et al. used metal-oxygen bond formation energies to predict the catalytic activity of different metal nodes. Here, we perform quantum mechanical calculations to test the applicability of such predictive descriptor on catalytic activity of unsaturated metal nodes in 2D MOFs. To be able to provide a gen-

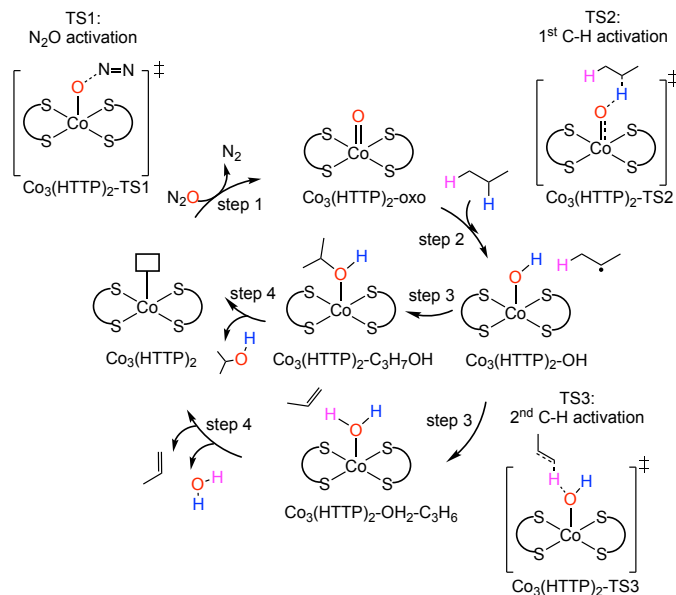


Fig. 3 Proposed mechanistic scheme for oxidative dehydrogenation of propane to propene (outside circle) or propanol (inside circle) using the coordinatively unsaturated open Co sites and N_2O as the oxidizing agent.²³

eral picture, we cut cluster models from optimized structures of both $M_3(HTTP)_2$ and $M_3(HHTTP)_2$ MOFs (with $M = Co$ and Cu) and truncate the organic linkers to dithiophenolates (DTP) and catecholates (CAT), respectively. The binding energy of oxygen to the open-metal sites, also referred to as metal-oxo bond formation energies (ΔE_O), were estimated relative to the bare node (E_M) and an isolated N_2O molecule (E_{N_2O}) using the following formula: $\Delta E_O = E_{M-O} + E_{N_2} - E_M - E_{N_2O}$. The N_2O activation barriers vs. the oxygen bond formation energies for these four cluster models are plotted in the SI Figure S7 which shows a very good correlation with $R^2 = 0.98$, validating the predictive tool suggested by Barona et al. in these systems. Notably, $Co(DTP)_2$ forms the most stable metal-oxo bond ($\Delta H_O = -62.6$ kcal/mol) and shows the lowest N_2O activation enthalpy of 30.4 kcal/mol.

Now, we look into utilizing the computed ΔE_O s as an energy descriptor to illustrate the degree of deformation and heterogeneity in 2D MOFs and also to explore if the correlation found between N_2O activation energy barriers and the ΔE_O s still holds. We take an ensemble approach by computing ΔE_O s for all 48 different catalytically active Co sites present in the $2 \times 2 \times 2$ $Co_3(HTTP)_2$ supercell with many local minima being surveyed for the framework. To account for temperature-induced structural transformations/deformations, these calculations were performed on the 293 K equilibrated MOF as well as for the 0 K optimized MOF for comparison.

Bonding of one oxygen atom to different open Co sites of the MD equilibrated $Co_3(HTTP)_2$ framework leads to formation of six different isomers which are shown in the middle panel of Figure 4. In the case of the 0 K optimized MOF, only four distinct isomers were identified, namely **Co**, **S**, **Co-S**, and **Co-Co(int)**. The two additional isomers in the MD equilibrated MOF, namely **Co-S(int)** and **Co-S(d)** are only formed due to the slipping of the

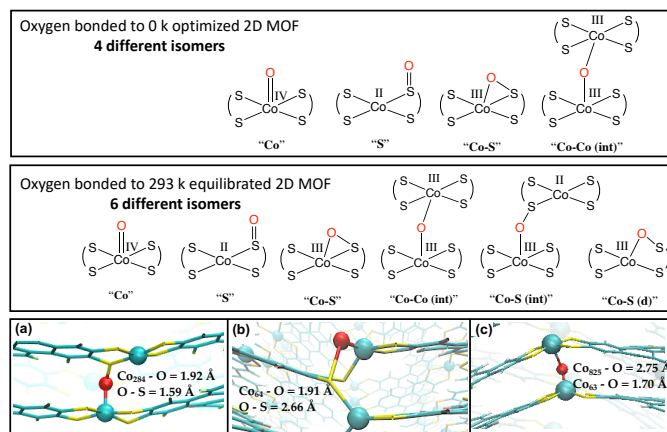


Fig. 4 Top: different active sites found for oxygen interacting with the 0 K and 293 K $Co_3(HTTP)_2$ frameworks where "int" stands for oxygen forming interlayer bonds and "d" stands for oxygen bonding to the defect sites present in the framework. Bottom: a, b, and c depict PBE-D3 optimized $Co_{284}-S(int)$, $Co_{64}-S(d)$, and $Co_{63}-Co_{825}(int)$ isomers, respectively. PBE-D3 computed metal-oxo bond formation energies and RESP charges of all 48 Co sites present in the 0 K and 293 K $Co_3(HTTP)_2$ frameworks are compiled in SI Tables S6 and S7. XYZ coordinates of all considered systems are provided as part of the ESI.

layers and deformation of the linkers as explained in the previous section. Starting from the 0 K optimized MOF, **Co** isomer was found to be the highest energy isomer with $\Delta E_O = 16.1$ kcal/mol followed by **Co-Co(int)**, **Co-S** and **S** isomers ($\Delta E_O = +1.3$, -20.0 , and -34.0 kcal/mol, respectively). This difference in ΔE_O s is likely due to changes in formal oxidation of Co upon binding to the oxygen atom from +2 to +4. In contrast, in the more stable **Co-S** and **S** isomers, due to the participation of the redox-active HTTP linkers, formal oxidation of Co increases only from +2 to +3 in the former and stays as +2 in the latter. Nevertheless, we classify the **S** isomers as off-cycle species that would not play a role in the reaction mechanism as depicted in Figure 3.

As can be seen from Figure 4b, incorporating temperature into simulations leads to creation of tetrahedral Co-sites coordinated to three HTTP linkers as opposed to nearly square planar geometry formed when it is bonded to two HTTP linkers (i.e. (a) and (c) in Figure 4). Out of 24 Co sites present inside the main 1D channel of the studied $2 \times 2 \times 2$ super cell, 8 fall into the category of tetrahedral sites which are amongst the most favorable sites for bonding to oxygen ($\Delta E_O = -47.1$ kcal/mol compared to -23.1 kcal/mol for the rest, SI Table S7). Computed RESP charges showed that these sites are more positively charged than the rest, with an average of $+0.473e$ vs. $+0.264e$ (SI Table S7). The computed ΔE_O values for **Co**, **Co-Co(int)**, and **Co-S** isomers in 293 K equilibrated MOF are 29.1, 22.4, and 5.7 kcal/mol, compared to the same isomers in the 0 K optimized MOF. When averaged over all 48 open- Co^{2+} sites, this value is found to be 26.1 kcal/mol lower than the corresponding value for the optimized system (-27.0 kcal/mol vs. -0.9 kcal/mol) indicating likely higher catalytic activity than what would be presumed based on *static* electronic structure calculations. These results highlight the importance of incorporating temperature which leads to structural deformation when studying catalysis in these fluxional materials.

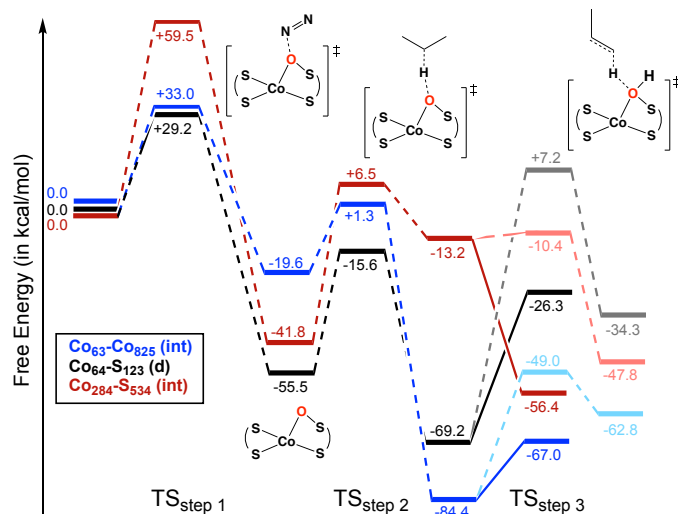


Fig. 5 M06-2X/def2-TZVP computed mechanistic scheme for the Co₆₃-Co₈₂₅(int), Co₆₄-S₁₂₃(d) and Co₂₈₄-S₅₃₄(int) sites. The unfavorable second C-H activation step leading to the formation of propene is highlighted with different colors. For clarity, only transition states for the Co₆₄-S₁₂₃(d) sites are shown.

Finally, we examined the four step mechanistic scheme, as outlined in Figure 3, for three representative isomers namely Co₆₃-Co₈₂₅(int), Co₆₄-S₁₂₃(d) and Co₂₈₄-S₅₃₄(int) (Figure 5). In the adopted nomenclature, numbers refer to the atom label of the Co centers in the considered 2×2×2 supercell. These Co centers experience different electronic environments and as such are expected to show different catalytic activity. The Co₆₄-S₁₂₃(d), a tetrahedral Co-site, shows the highest ΔE_O as well as the lowest activation free energy (ΔG^\ddagger) of 29.2 kcal/mol for **step 1**. However, **step 2**, i.e. the first C-H activation step, is found to be the rate-limiting step for this active site. The Co₂₈₄-S₅₃₄(int) isomer which has a higher ΔE_O than the Co₆₃-Co₈₂₅(int) (-41.8 kcal/mol vs. -19.6 kcal/mol) shows the lowest reactivity among all (with ΔG^\ddagger values of 59.5 kcal/mol vs. 33.0 kcal/mol in Co₆₃-Co₈₂₅(int)). Interestingly, all studied Co active sites show higher propensity toward formation of propanol than propene (Figure 5).

Overall, we show for the first time that incorporation of intrinsic temperature-induced structural deformations in 2D MOFs is crucial in realization of some of the most catalytically active Co²⁺ sites toward oxidative dehydrogenation of propane to propanol. These active sites are only formed when slipping movement of the layers and twisting motion of the organic linkers are considered in the simulations. We believe these findings are a step forward in providing structure-to-function design guidelines for flexible materials such as the 2D MOFs studied in this work. Future works are directed toward screening of both synthesized and potential 2D layered MOFs with various coordinatively unsaturated metal sites, aiming at enhancing their catalytic activity.

Acknowledgement

This work is supported by start-up funds from NJIT and used the Extreme Science and Engineering Discovery Environment (XSEDE) which is supported by NSF grant numbers CHE200007

and CHE200008. This research has been (partially) enabled by the use of computing resources provided by the NJIT's HPC center KONG. We thank Prof. Christopher J. Cramer, and Drs Manuel Ortuno, David Dell'Angelo, Sandra Brown, Xuan Zhang, and Xingjie Wang for critically reading this manuscript.

Conflicts of interest

There are no conflicts to declare.

Notes and references

- D. Sheberla, L. Sun, M. A. Blood-Forsythe, S. Er, C. R. Wade, C. K. Brozek, A. Aspuru-Guzik and M. Dinca, *J. Am. Chem. Soc.*, 2014, **136**, 8859–8862.
- G. Wu, J. Huang, Y. Zang, J. He and G. Xu, *J. Am. Chem. Soc.*, 2017, **139**, 1360–1363.
- M. E. Foster, K. Sohlberg, M. D. Allendorf and A. A. Talin, *J. Phys. Chem. Lett.*, 2018, **9**, 481–486.
- W.-H. Li, K. Ding, H.-R. Tian, M.-S. Yao, B. Nath, W.-H. Deng, Y. Wang and G. Xu, *Adv. Funct. Mater.*, 2017, **27**, 1702067.
- M. Hmadeh, Z. Lu, Z. Liu, F. Gándara, H. Furukawa, S. Wan, V. Augustyn, R. Chang, L. Liao, F. Zhou, E. Perre, V. Ozolins, K. Suenaga, X. Duan, B. Dunn, Y. Yamamoto, O. Terasaki and O. M. Yaghi, *Chem. Mater.*, 2012, **24**, 3511–3513.
- L. Sun, M. G. Campbell and M. Dincă, *Angew. Chem. Int. Ed.*, 2016, **55**, 3566–3579.
- M. Ko, L. Mendecki and K. A. Mirica, *Chem. Commun.*, 2018, **54**, 7873–7891.
- M. K. Smith, K. E. Jensen, P. A. Pivak and K. A. Mirica, *Chem. Mater.*, 2016, **28**, 5264–5268.
- D. Sheberla, J. C. Bachman, J. S. Elias, C.-J. Sun, Y. Shao-Horn and M. Dincă, *Nat. Mater.*, 2017, **16**, 220–224.
- S. Chen, J. Dai and X. C. Zeng, *Phys. Chem. Chem. Phys.*, 2015, **17**, 5954–5958.
- M. Ko, L. Mendecki, A. M. Eagleton, C. G. Durbin, R. M. Stolz, Z. Meng and K. A. Mirica, *J. Am. Chem. Soc.*, 2020, **142**, 11717–11733.
- K. W. Nam, S. S. Park, R. dos Reis, V. P. Dravid, H. Kim, C. A. Mirkin and J. F. Stoddart, *Nat. Commun.*, 2019, **10**, 4948.
- L. Mendecki and K. A. Mirica, *ACS Appl. Mater. Interfaces*, 2018, **10**, 19248–19257.
- M.-S. Yao, X.-J. Lv, Z.-H. Fu, W.-H. Li, W.-H. Deng, G.-D. Wu and G. Xu, *Angew. Chem. Int. Ed.*, 2017, **56**, 16510–16514.
- Y. Shi, M. R. Momeni, Y.-J. Chen, Z. Zhang and F. A. Shakib, *Chem. Mater.*, 2020, **32**, 9664–9674.
- M. R. Momeni and C. J. Cramer, *ACS Appl. Mater. Interfaces*, 2018, **10**, 18435–18439.
- M. R. Momeni and C. J. Cramer, *Chem. Mater.*, 2018, **30**, 4432–4439.
- M. R. Momeni and C. J. Cramer, *J. Phys. Chem. C*, 2019, **123**, 15157–15165.
- D. Yang, M. R. Momeni, H. Demir, D. R. Pahls, M. Rimoldi, T. C. Wang, O. K. Farha, J. T. Hupp, C. J. Cramer, B. C. Gates and L. Gagliardi, *Faraday Discuss.*, 2017, **201**, 195–206.
- M. Kalaj, M. R. Momeni, K. C. Bentz, K. S. Barcus, J. M. Palomba, F. Paesani and S. M. Cohen, *Chem. Commun.*, 2019, **55**, 3481–3484.
- Z. Li, A. W. Peters, V. Bernales, M. A. Ortuno, N. M. Schweitzer, M. R. DeStefano, L. C. Gallington, A. E. Platero-Prats, K. W. Chapman, C. J. Cramer, L. Gagliardi, J. T. Hupp and O. K. Farha, *ACS Cent. Sci.*, 2017, **3**, 31–38.
- M. D. Korzynski and M. Dinca, *ACS Cent. Sci.*, 2017, **3**, 10–12.
- M. Barona, S. Ahn, W. Morris, W. Hoover, J. M. Notestein, O. K. Farha and R. Q. Snurr, *ACS Cat.*, 2020, **10**, 1460–1469.
- M. Barona and R. Q. Snurr, *ACS Appl. Mater. Interfaces*, 2020, **12**, 28217–28231.
- T. Nobukawa, M. Yoshida, S. Kameoka, S.-i. Ito, K. Tomishige and K. Kunimori, *J. Phys. Chem. B*, 2004, **108**, 4071–4079.
- B. Ipek and R. F. Lobo, *Chem. Commun.*, 2016, **52**, 13401–13404.
- A. Zecchina, M. Rivallan, G. Berlier, C. Lamberti and G. Ricchiardi, *Phys. Chem. Chem. Phys.*, 2007, **9**, 3483–3499.
- P. Verma, K. D. Vogiatzis, N. Planas, J. Borycz, D. J. Xiao, J. R. Long, L. Gagliardi and D. G. Truhlar, *J. Am. Chem. Soc.*, 2015, **137**, 5770–5781.
- Z.-J. Zhao, A. Kulkarni, L. Vilella, J. K. Nørskov and F. Studt, *ACS Cat.*, 2016, **6**, 3760–3766.
- N. Mardirossian and M. Head-Gordon, *J. Chem. Phys.*, 2016, **144**, 214110.
- X. Sun, K.-H. Wu, R. Sakamoto, T. Kusamoto, H. Maeda, X. Ni, W. Jiang, F. Liu, S. Sasaki, H. Masunaga and H. Nishihara, *Chem. Sci.*, 2017, **8**, 8078–8085.
- A. Clough, J. Skelton, C. Downes, A. de la Rosa, J. Yoo, A. Walsh, B. Melot and S. Marinescu, *J. Am. Chem. Soc.*, 2017, **139**, 10863–10867.
- J.-H. Dou, L. Sun, Y. Ge, W. Li, C. Hendon, J. Li, S. Gul, J. Yano, E. Stach and M. Dincă, *J. Am. Chem. Soc.*, 2017, **139**, 13608–13611.
- W. Li, L. Sun, J. Qi, P. Jarillo-Herrero, M. Dinca and J. Li, *Chem. Sci.*, 2017, **8**, 2859–2867.